

# STRUCTURE OF PROTON COMPONENT OF NEUTRON STAR MATTER FOR REALISTIC NUCLEAR MODELS

M. KUTSCHERA<sup>a,b</sup>, S. STACHNIEWICZ<sup>a</sup>,  
A. SZMAGLIŃSKI<sup>c</sup> AND W. WÓJCIK<sup>c</sup>

<sup>a</sup> H. Niewodniczański Institute of Nuclear Physics,  
ul. Radzikowskiego 152, 31-342 Kraków, Poland

<sup>b</sup> Institute of Physics, Jagiellonian University,  
ul. Reymonta 4, 30-059 Kraków, Poland

<sup>c</sup> Institute of Physics, Technical University,  
ul. Podchorążych 1, 30-084 Kraków, Poland

We study properties of the proton component of neutron star matter for a number of realistic nuclear models. Protons which form a few percent admixture tend to be localized in potential wells corresponding to neutron matter inhomogeneities created by the protons in the neutron medium. We calculate the energy of the Wigner-Seitz cell enclosing a single localized proton. The neutron background is treated in the Thomas-Fermi approximation and the localized proton is described by the Gaussian wave function. The neutron density profile is obtained by solving the appropriate variational equation. This approach gives lower energies of localized protons than obtained previously with less sophisticated methods.

PACS numbers: 21.65.+f, 97.60.Jd

## 1. Introduction

Physical properties of the neutron star interior relevant to macroscopic observables are rather sensitive to the microscopic structure of dense nuclear matter in neutron stars. For example, the transport and magnetic properties of neutron stars depend strongly on the structure of the so called liquid core. Particularly important is the structure of the proton component. A uniform proton distribution and a periodic (crystalline) proton arrangement result in very different properties [1]. The latter possibility was discussed in Refs. [2, 3] for strongly asymmetric nuclear matter which was shown to be unstable with respect to proton localization. The localization effect is a result of the interaction of protons with small density

oscillations of the neutron background [4]. The protons behave as localized polarons which form a periodic lattice at high densities [5].

The presence of the localized protons inside neutron star cores would have profound astrophysical consequences. The transport properties of such a phase are rather different from that of a uniform nuclear matter [6]. In particular, the cooling proceeds in a quite different way. Recent analysis [6] shows that the presence of such localized proton phase results in more satisfactory fits of temperatures of observed neutron stars. Also, spin ordering of localized protons could strongly affect magnetic properties of the system [2, 7]. The spin ordered phase can contribute significantly to the observed magnetic moments of neutron stars [8, 9].

The aim of this paper is to study the proton localization for a number of realistic nuclear models with improved variational method. In original calculations [3, 4] both the proton wave function and the neutron density distribution were assumed to be trial functions which included variational parameters. In this paper we find better estimates of energies of localized protons by solving the appropriate variational equation for the neutron density profile that gives the minimum energy for a fixed wave function of the localized proton.

The paper is organized as follows: In the next section we describe the model of proton impurities in the neutron star matter. In Sect.3 simple estimates of the proton localization based on trial functions are given. Sect.4 contains the formulation and the solution of the variational problem. Results are discussed in Sect.5.

## 2. Model of proton impurities in the neutron star matter

The amount of protons present in the neutron star matter, which is charge neutral and  $\beta$ -stable, is crucial for the cooling rate of neutron stars and also plays an important role for magnetic and transport properties of neutron star matter. Nuclear models do not uniquely predict the proton fraction of the neutron star matter at high densities. This controversy is discussed in details in Ref. [1, 10] where the discrepancy of the proton fraction in various models is shown to reflect the uncertainty of the nuclear symmetry energy at high densities. In this paper we consider a class of nuclear interaction models for which the proton fraction is of the order of a few percent and decreases at high densities - as shown in Fig.1. For the calculations we have chosen six realistic nuclear interaction models. These are interactions derived by Myers and Swiatecki [11](MS), the Skyrme potential with parameters from Ref. [12, 13] (Sk), the Friedman and Pandharipande interactions [14] (as parametrized by Ravenhall in Ref.[15]) (FPR) and three models, UV14+TNI, AV14+UVII and UV14+UVII, from

Ref.[16] by Wiringa et al.

Let us consider a neutron star matter containing a small proton fraction  $x$ . To compare the energy of a normal phase of uniform density and a phase with localized protons we apply the Wigner-Seitz approximation and divide the system into cells, each of them enclosing a single proton [2, 4]. For simplicity, the cells are assumed to be spherical. The volume of the cell is  $V = 1/n_P$ . The normal phase is of uniform density  $n_N$  and the neutron chemical potential is  $\mu_N$ . In the uniform density phase protons are not localized and their wave functions are plane waves.

The energy of the cell, which is a sum of proton and neutron energies, reads

$$E_0 = V\epsilon(n_N, n_P), \quad (1)$$

where  $\epsilon(n_N, n_P)$  is the energy density of the uniform phase. For small proton density, i.e. for low  $x$ , we can expand the energy density

$$\epsilon(n_N, n_P) \approx \epsilon(n_N, 0) + \mu_P(n_N, 0) n_P. \quad (2)$$

In the following we shall adopt abbreviations  $\epsilon(n_N) = \epsilon(n_N, 0)$  for the energy density of pure neutron matter and  $\mu_P(n_N) = \mu_P(n_N, 0)$  for the proton chemical potential in pure neutron matter. The energy of the cell is thus approximately

$$E_0 = \mu_P(n_N) + V\epsilon(n_N). \quad (3)$$

Our aim is to compare the energy of the normal phase, where protons are nonlocalized, with the energy of a phase where the protons are trapped into potential wells, corresponding to the nonuniform neutron density distribution, which most likely form a regular arrangement. We treat this proton "crystal" in the Wigner-Seitz approximation.

Let us consider a Wigner-Seitz cell with nonuniform neutron matter distribution  $n(r)$  surrounding the proton whose wave function is  $\Psi_P$ . In the local density approximation one can identify the proton effective potential with the local proton chemical potential  $\mu_P(n)$  [2]. The proton's effective potential varies locally with neutron matter density  $n(r)$ . This results in a potential well  $\mu_P(n(r))$  which affects the single proton wave function. The energy of the Wigner-Seitz cell,  $E_L$ , is:

$$\begin{aligned} E_L = \int_V \{ \Psi_P^*(r) \left[ -\frac{\nabla^2}{2m_P} + \mu_P(n(r)) \right] \Psi_P(r) \\ + \epsilon(n(r)) + B_N \left( \vec{\nabla} n(r) \right)^2 \} d^3r. \end{aligned} \quad (4)$$

The first term is the energy of the proton in the effective potential  $v_{eff}(r) = \mu_P(n(r))$ . It is by construction the attractive potential well. At high densities the derivative of the proton chemical potential is positive,  $\frac{\partial \mu_P}{\partial n} > 0$ , for all interactions we use. This can be seen in Fig.2 where the proton chemical potential in pure neutron matter is shown for nuclear interaction models from Fig.1. The neutron density profile  $n(r)$  is thus assumed to have a minimum at the center of the cell.

The two other terms in eq.(4) describe the neutron background contributions to the energy. These represent the neutron Fermi sea energy and the curvature energy due to the gradient of the neutron distribution, respectively, in the Thomas-Fermi approximation. Here  $\epsilon(n(r))$  is the local neutron matter energy per unit volume. The parameter  $B_N$  is the curvature coefficient for pure neutron matter [2].

To decide which is the ground state configuration we compare the energies  $E_0$  and  $E_L$  assuming the same number of neutrons in the cell. This means that the neutron density variation conserves the baryon number:

$$\int_V (n(r) - n_N) d^3r = 0. \quad (5)$$

In the next section the minimum of the energy difference  $\Delta E = E_L - E_0$  is calculated in a simple variational approach and in Sect.4 more sophisticated method is developed.

### 3. Simple estimate of the localized proton energy

We assume a simple trial form of the proton wave function and the neutron density variation. For the proton wave function we use a Gaussian form:

$$\Psi_P(r) = \left(\frac{2}{3}\pi R_P^2\right)^{-\frac{3}{4}} \exp\left(-\frac{3}{4}\frac{r^2}{R_P^2}\right). \quad (6)$$

Here  $R_P$  is the rms radius of the localized proton probability distribution. We treat this quantity as a variational parameter and minimize the energy difference  $\Delta E$  with respect to  $R_P$ .

Using the trial form of the proton wave function  $\Psi_P(r)$  the energy difference  $\Delta E$  becomes

$$\begin{aligned} \Delta E = & \frac{9}{8m_P R_P^2} + \int_V \{ \Psi_P^2(r) (\mu_P(n(r)) - \mu_P(n_N)) + \\ & \epsilon(n(r)) - \epsilon(n_N) + B_N \left(\frac{dn(r)}{dr}\right)^2 \} d^3r. \end{aligned} \quad (7)$$

The neutron density  $n(r)$  is chosen to be [2, 4]:

$$n(r) = n_N + \alpha \left[ \Psi_P^*(r) \Psi_P(r) - \frac{1}{V} \right]. \quad (8)$$

Here  $\alpha$  is the second variational parameter;  $\alpha > 0$  corresponds to the neutron density enhancement around the proton and  $\alpha < 0$  corresponds to the bubble in the neutron density near the proton.

We calculate the energy difference  $\Delta E$ , Eq.(7), for small proton fraction  $x$ , i. e. in the limit of large volume  $V$ . The first and the last terms were calculated assuming that the Wigner-Seitz cell radius  $R_C$  is much bigger than  $R_P$ ,  $R_C \gg R_P$ . Denoting  $\Psi_P^*(r) \Psi_P(r) = p(r)$  and expanding in  $\frac{1}{V}$  we have

$$\begin{aligned} \int_V p(r) \left( \mu_P \left( n_N + \alpha p(r) - \alpha \frac{1}{V} \right) - \mu_P(n_N) \right) d^3r = \\ \int_V p(r) (\mu_P(n_N + \alpha p(r)) - \mu_P(n_N)) d^3r - \\ \alpha \frac{1}{V} \int_V p(r) \frac{\partial \mu_P}{\partial n} (n_N + \alpha p(r)) d^3r. \end{aligned} \quad (9)$$

The integral in the last term does not depend on the cell volume so that this term vanishes in the limit  $V \rightarrow \infty$ . Expanding in the same way the energy density, we obtain from the third term in Eq.(7)

$$\begin{aligned} \int_V \left[ \epsilon \left( n_N + \alpha p(r) - \alpha \frac{1}{V} \right) - \epsilon(n_N) \right] d^3r = \\ \int_V [\epsilon(n_N + \alpha p(r)) - \epsilon(n_N)] d^3r - \alpha \mu_N(n_N) - \\ \alpha \frac{1}{V} \int_V (\mu_N(n_N + \alpha p(r)) - \mu_N(n_N)) d^3r. \end{aligned} \quad (10)$$

Here also the integral in the last term does not depend on the cell volume, since  $p(r)$  is a Gaussian, and this term vanishes for large  $V$ . The last term containing the coefficient of curvature  $B_N$  is easily evaluated to be:

$$\int_V B_N \left( \vec{\nabla} n(r) \right)^2 d^3r = \frac{9}{2} \left( \frac{4}{3} \pi \right)^{-\frac{3}{2}} \frac{1}{R_P^5} B_N \alpha^2. \quad (11)$$

The energy difference  $\Delta E$  thus becomes:

$$\Delta E = \frac{9}{8m_P R_P^2} + \int_V \{ (\mu_P(n(r)) - \mu_P(n_N)) p(r) \} d^3r +$$

$$\int_V \{\epsilon(n(r)) - \epsilon(n_N)\} d^3r - \alpha \mu_N(n_N) + \frac{9}{2} \left(\frac{4}{3}\pi\right)^{-\frac{3}{2}} \frac{1}{R_P^5} B_N \alpha^2. \quad (12)$$

We obtain physical parameters of the localized phase for a given neutron matter density  $n_N$  by a straightforward minimization of  $\Delta E$  with respect to the two variational parameters  $\alpha$  and  $R_P$ .

The results of the calculations for the MS and FPR nuclear interactions are presented, respectively, in Figs.3 and 4 where we show the energy difference  $\Delta E$  as a function of the proton distribution rms radius  $R_P$  for a few values of the neutron density. The curves are labeled with the value of the neutron matter density  $n_N$  with subscript  $\alpha$ . One can notice that for both MS and FPR interactions there appears a local minimum above a certain density, for the proton rms radius  $R_P$  in the range  $1fm - 2fm$ . We have chosen the results for MS and FPR interactions only as examples of a general behaviour which is observed for all interactions we use in the calculations (more detailed account of our calculations will be presented elsewhere). With increasing neutron matter density  $n_N$  the depth of the minimum increases and above the threshold density the energy difference becomes negative. The negative value  $\Delta E < 0$  means that the energy of the localized proton is lower than the energy of a nonlocalized proton and the localized proton state is preferred energetically. The behaviour of  $\Delta E$  is very similar for all interactions we examine. This shows that the localization is not an effect of some specific interaction but rather is a general qualitative feature of the physical system we consider. Quantitative results, i. e. the localization density, the value of  $\Delta E$  at the minimum and the localization radius  $R_P$ , depend on the specific interactions. The proton localization occurs at the lowest density for the Skyrme interactions,  $n_{loc} = 0.4fm^{-3}$ , and the energy difference  $\Delta E$  displays the fastest decrease with the density. One can say that the localization is the strongest in this case.

To understand better the localization mechanism it seems useful to consider separately various contributions to the total energy difference. In Figs.5 and 6 we show the proton contribution,  $E_P$ , to the energy difference  $\Delta E$ , which consists of kinetic and potential terms. Here the minimum occurs at lower values of the proton rms radius  $R_P$ . One should keep in mind that the proton energy contribution represents a difference of the kinetic and potential energies of a localized proton and a single plane-wave proton. In the latter case the kinetic energy is zero. Next figures, Figs.7 and 8, show the contribution of the neutron background to the total energy difference. This contribution is a monotonically decreasing function of the proton rms radius  $R_P$ . It grows very fast for low values of  $R_P$ . This rapid growth is similar to the behaviour of the gradient term contribution which is displayed in Figs.9 and 10. Thus a sum of these contributions also grows fast for low values

of  $R_P$ . Its values for a given radius  $R_P$  increase with the mean neutron density  $n_N$ .

The minimum of the total energy difference,  $\Delta E$ , which is a sum of all contributions shown in Figs.5-10, is thus a result of a delicate balance between repulsive contributions due to the neutron background, the proton kinetic term and the neutron curvature energy, and the attractive part of the proton interaction energy. Results of our calculations for a number of effective nuclear interactions show that such a minimum occurs in all cases above some density. One may thus conclude that the localization of proton impurity in the neutron matter is a general prediction of nuclear models of the class we consider here.

The threshold density for proton localization,  $n_{loc}$ , depends also on the curvature coefficient  $B_N$  entering the gradient term and the proton effective mass  $m_P$ , which are parameters of our model. In Fig.11 we show how  $n_{loc}$  changes with  $B_N$ . One can notice that the localization density only weakly increases with the curvature coefficient in a wide range of its values. Also, the rms proton distribution radius at the threshold density  $R_P^{loc}$  increases slowly with increasing curvature coefficient  $B_N$ , Fig.12. This fact is rather important in regard of validity of the Thomas-Fermi approach used in our model.

The threshold density  $n_{loc}$  depends in a more sensitive way on the proton effective mass,  $m_P$ , as shown in Fig.13. For values of  $m_P$  less than the bare proton mass the localization density increases. However, in the range  $600\text{MeV} - 938\text{MeV}$  which is most likely physically relevant to neutron stars, the threshold density changes by about 20%.

#### 4. The self-consistent method

Variational calculations of the localized proton energy presented in the previous section used the trial functions with only two variational parameters,  $\alpha$  and  $R_P$ . In this section we develop more advanced variational method which should give better estimate of the ground state energy of a localized proton.

The energy difference  $\Delta E$ , is a functional of two functions  $\Psi(r)$  and  $n(r)$ . The physical constraint is that the variation of the neutron background conserves the baryon number. We should thus look for such functions  $\Psi(r)$  and  $n(r)$  that minimize the functional

$$f[n(r), \Psi_P(r)] = \Delta E - \lambda \int_V [n(r) - n_N] d^3r - E \left[ \int_V \Psi_P^*(r) \Psi_P(r) d^3r - 1 \right], \quad (13)$$

where we explicitly include constraints of the baryon number conservation, Eq.(14), and the proton wave function normalization

$$\int_V \Psi_P^*(r) \Psi_P(r) d^3r - 1 = 0. \quad (14)$$

The Euler-Lagrange equations corresponding to the functional (13) can be found easily. The differentiation with respect to  $\Psi_P^*$  gives the Schrödinger equation for the proton impurity:

$$-\frac{1}{2m_P} \nabla^2 \Psi_P(r) + [\mu_P(n(r)) - \mu_P(n_N)] \Psi_P(r) = E_P \Psi_P(r). \quad (15)$$

Differentiation with respect to  $n(r)$  gives the second-order equation for the neutron density distribution  $n(r)$ :

$$\frac{\partial \mu_P(n(r))}{\partial n(r)} \Psi_P^*(r) \Psi_P(r) + \mu_N(n(r)) + 2B_N \frac{d^2 n(r)}{dr^2} - \lambda = 0. \quad (16)$$

The boundary conditions the functions  $\Psi(r)$  and  $n(r)$  obey at  $r \rightarrow \infty$  are:  $n(r) = n_N$ ,  $|\Psi_P(r)|^2 = 0$ . This allows us to identify the Lagrange multiplier  $\lambda$  with the neutron chemical potential,

$$\lambda = \mu_N(n_N). \quad (17)$$

To calculate the cell energy we adopt for the proton wave function the Gaussian form used in the previous section and solve with this ansatz the equation (16). The rms radius of the proton probability distribution,  $R_P$ , is treated as a variational parameter. Numerical solutions of eq.(16) are presented in Figs.14 and 15, where we show the neutron density distributions  $n(r)$  obtained from equation (16). As one can notice the neutron background has somewhat different shape than that used in Sect.3. In particular, at higher mean neutron densities  $n_N$  there appears a significant density enhancement at the well boundary which considerably strengthens the localization effect. With the simple method of Sect.3 the neutron distribution around the proton is a monotonically increasing function of the radius.

Results of calculations of the energy difference  $\Delta E$  with the self-consistent method are presented in Figs.3 and 4 as curves labeled with the value of the neutron matter density only. In Figs.5 - 10 the proton contribution and all components of the neutron background contribution to the full energy difference are shown together with those obtained in Sect.3. The neutron background energy, Figs. 7 and 8, calculated with the self-consistent method



is well below the simple estimate of Sect.3 for low values of the proton distribution radius  $R_P$ . The reduction of the energy is even bigger for the gradient term contribution, Figs.9 and 10. An opposite effect is observed for the proton energy contribution, Figs. 5 and 6, where the energy corresponding to the self-consistent method is higher than that calculated with simple trial functions in Sect.3.

## 5. Conclusions and implications

Our self-consistent method gives lower energies of localized protons than the variational method used in sect.3. In Figs.3 and 4 we compare the energy difference  $\Delta E$  obtained with both methods, for the MS and FPR models of nuclear interactions. As functions of the radius  $R_P$  the energy differences  $\Delta E$  for the old variational method and for the selfconsistent method depart from one another only for small values of  $R_P$ . At  $R_P > 1fm$  the curves for both methods in Figs.3 and 4 are practically identical. However at small  $R_P$  the self-consistent method gives significantly lower energies. The minimum values of  $\Delta E$  are considerably below those found with the old method and they occur at somewhat smaller radii. Our study indicates also that with the growing curvature coefficient the localization density grows. The results presented in Fig.11 show that this growth is weak and the values corresponding to both methods are quite similar. Also, the dependence of the localization density on the proton effective mass, Fig.13 is very similar for both methods.

To conclude, the self-consistent calculations improve the estimate of the energy of the cell containing a localized proton, especially at small values of the rms proton radius  $R_P$ . The proton contribution  $E_P$  and the gradient term contribution to  $\Delta E$  are most affected by the new method. The ultimate goal is to calculate the proper wave function of the proton, which would give the true energy of the localized state.

Results of our calculations for nuclear interactions we use indicate that the proton impurity in neutron star matter becomes localized at densities above  $0.5 - 1.0fm^{-3}$ . The selfconsistent method gives lower energies of localized protons and smaller threshold localization densities than simple variational method with trial functions. This has important consequences for neutron stars as densities in this range correspond to inner core of neutron stars with masses exceeding one solar mass,  $M > 1M_\odot$ . In Fig. 16 we show neutron star masses corresponding to all nuclear interactions used in the calculations reported above.

## REFERENCES

- [1] M. Kutschera, Phys. Lett. B **340**, 1 (1994).
- [2] M. Kutschera and W. Wójcik, Acta Phys. Pol. **B21**, 823 (1990).
- [3] M. Kutschera and W. Wójcik, Phys. Lett. **223B**, 11 (1989).
- [4] M. Kutschera and W. Wójcik, Phys. Rev. **C47**, 1077 (1993).
- [5] M. Kutschera and W. Wójcik, Nucl. Phys. **A581**, 706 (1995).
- [6] D. A. Baiko and P. Haensel, Astron. Astrophys. **356**, 171 (2000).
- [7] M. Kutschera and W. Wójcik, Acta Phys. Pol. B **27**, 2227 (1996).
- [8] M. Kutschera, W. Wójcik, Acta Phys. Pol. B **B23**, 947 (1992).
- [9] M. Kutschera, MNRAS, **307**, 784 (1999).
- [10] M. Kutschera, Z. Phys. **A348**, 263 (1994).
- [11] W. D. Myers and W. J. Swiatecki, Acta Phys. Pol. B **26**, 111 (1995).
- [12] D. Vautherin and D. M. Brink, Phys. Lett. **32B**, 149 (1970).
- [13] D. G. Ravenhall, C.D. Bennett and C. J. Pethick, Phys. Rev. Lett. **28**, 978 (1972).
- [14] B. Friedman and V. R. Pandharipande, Nucl. Phys. **A361**, 502 (1981).
- [15] J. M. Lattimer, Ann. Rev. Nucl. Part. Sci. **31**, 337 (1981).
- [16] R. W. Wiringa, V. Fiks and A. Fabrocini, Phys. Rev. **C38**, 1010 (1988).

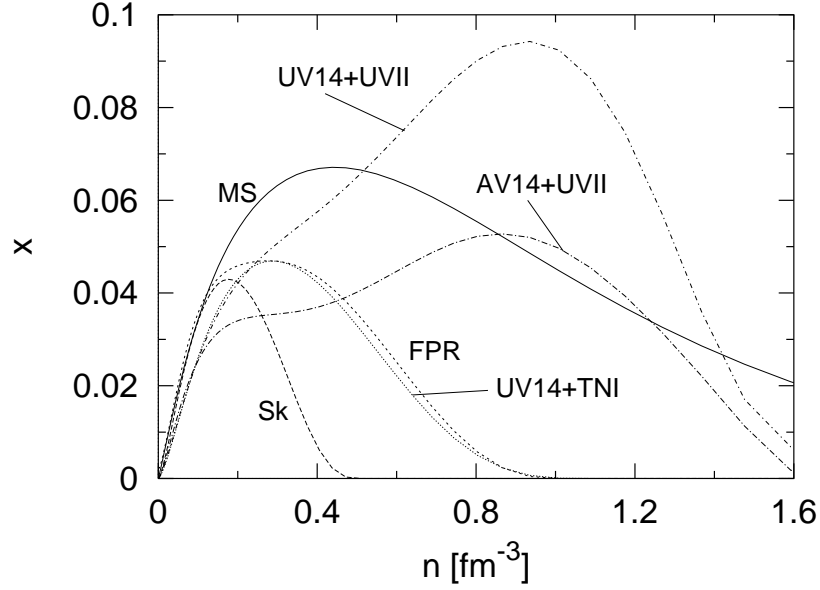


Fig. 1. The proton fraction of the neutron star matter as a function of baryon number density for indicated nuclear interaction models.

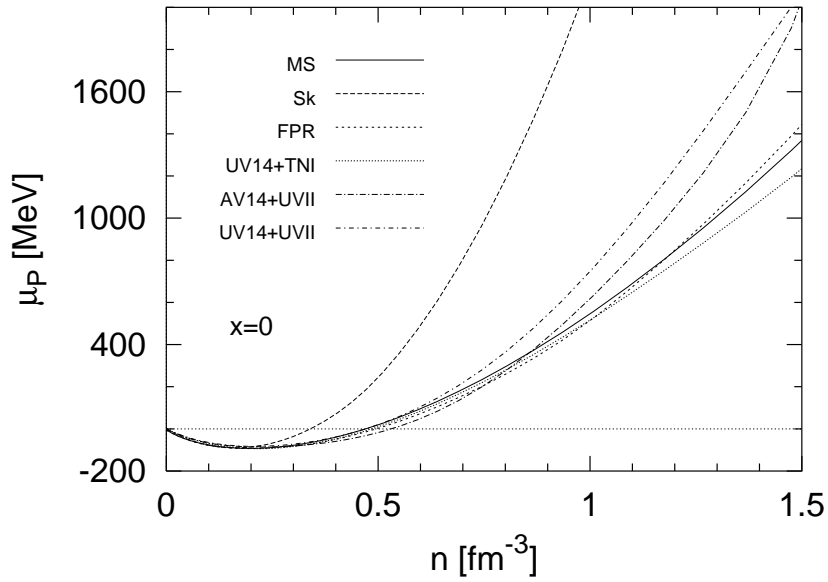


Fig. 2. The proton chemical potential in pure neutron matter as a function of baryon number density for the same interactions as in Fig.1.

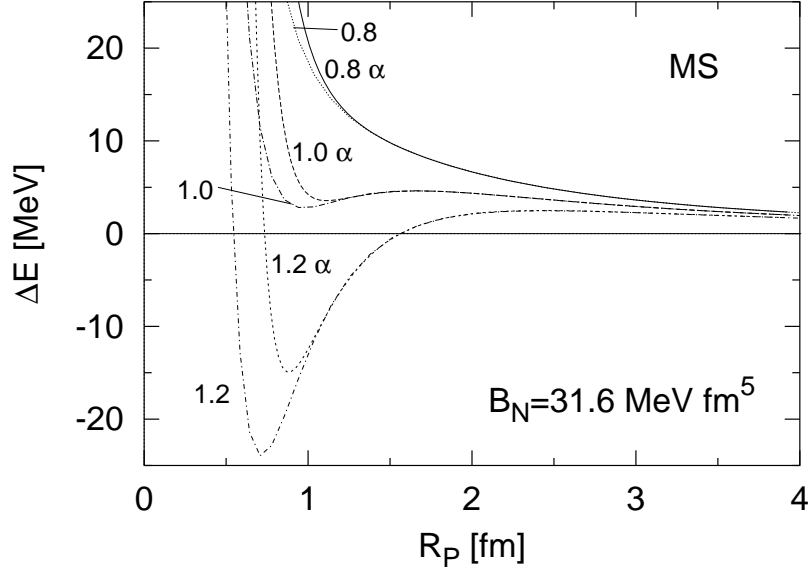


Fig. 3. The energy difference  $\Delta E$  as a function of the proton rms radius for the Myers and Swiatecki interaction. The curves corresponding to the self-consistent calculations are labeled with the value of the neutron matter density in  $[\text{fm}^{-3}]$ . The curves labeled additionally with the letter  $\alpha$  correspond to the simple method of Sect. 3.

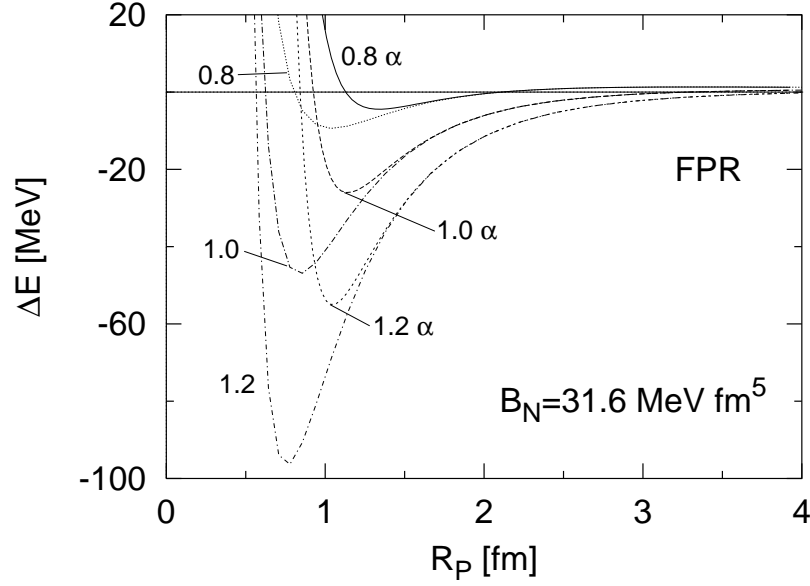


Fig. 4. The same as in Fig.3 for the Friedman-Pandharipande-Ravenhall nuclear interaction.

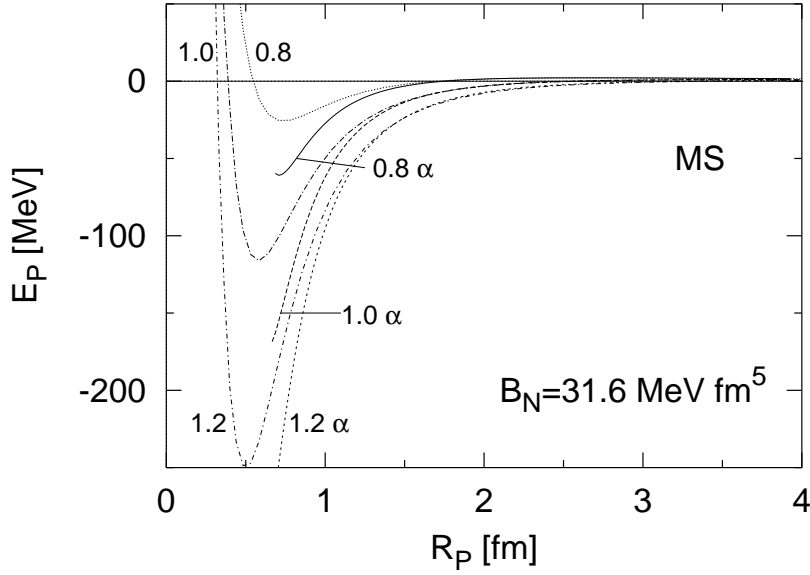


Fig. 5. The proton contribution to  $\Delta E$  for the Myers and Swiatecki model of nuclear interactions. Curves labeled as in Fig.3.

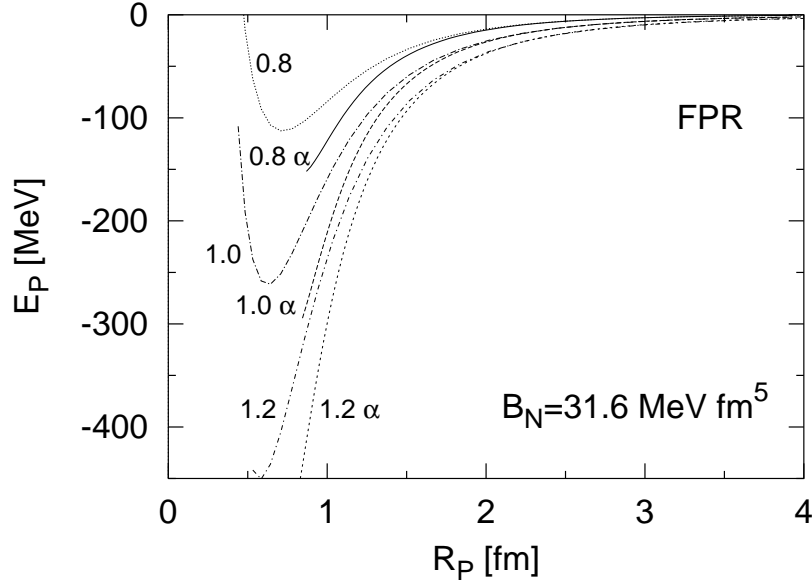


Fig. 6. The same as in Fig.5 for the Friedman-Pandharipande-Ravenhall interactions.

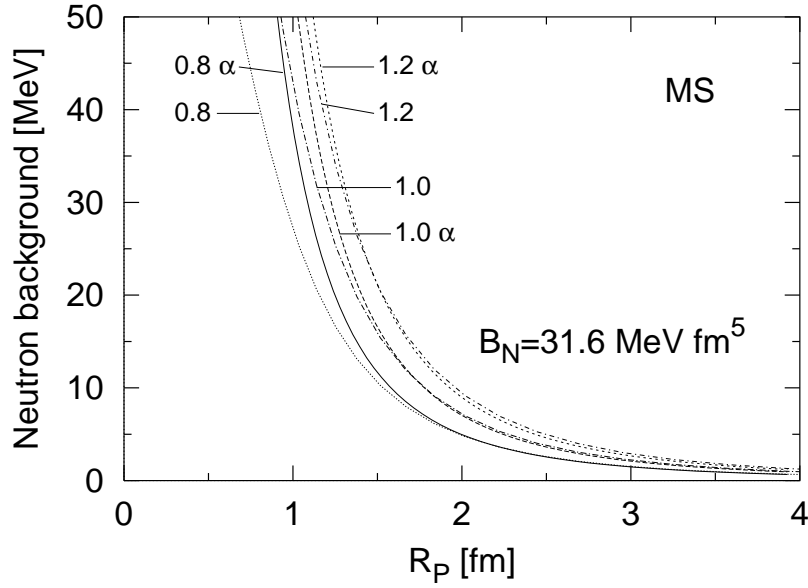


Fig. 7. The neutron background contribution to  $\Delta E$  for the Myers and Swiatecki model of nuclear interactions. Curves labeled as in Fig.3

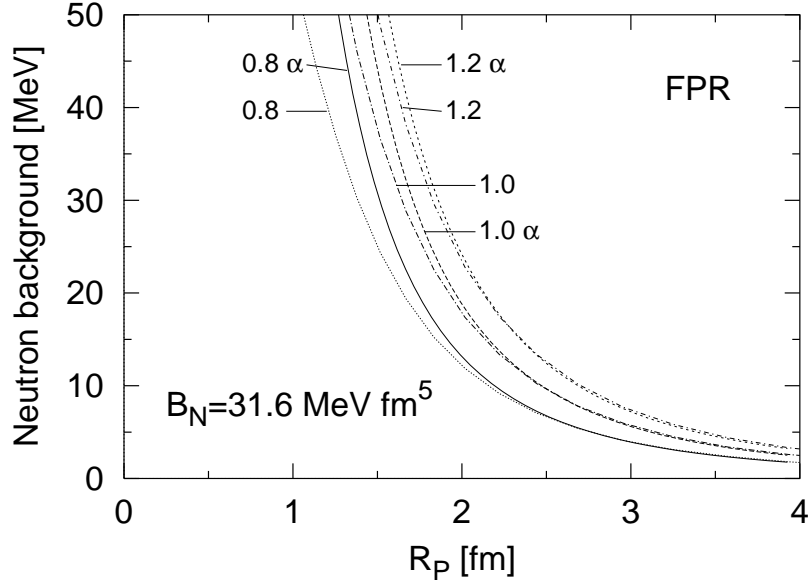


Fig. 8. The same as in Fig.7 for the Friedman-Pandharipande-Ravenhall interaction.

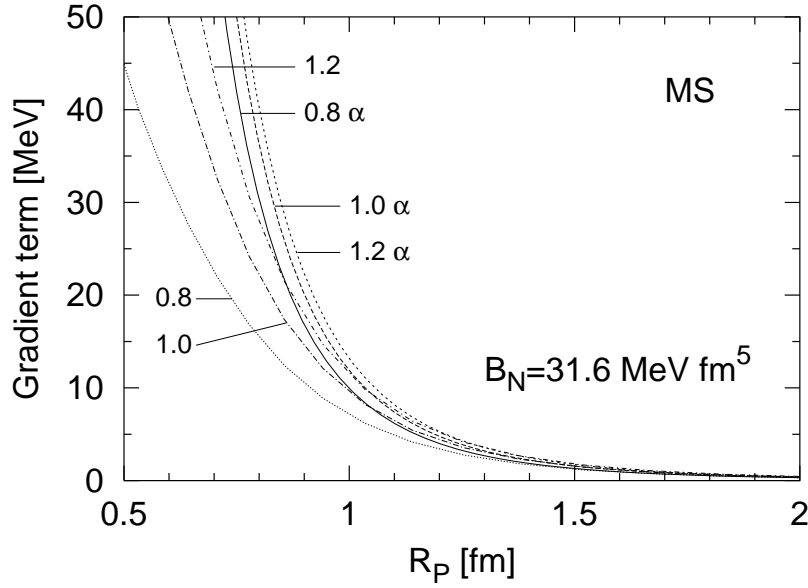


Fig. 9. The gradient term contribution to  $\Delta E$  for the Myers and Swiatecki nuclear interactions. Curves labeled as in Fig.3

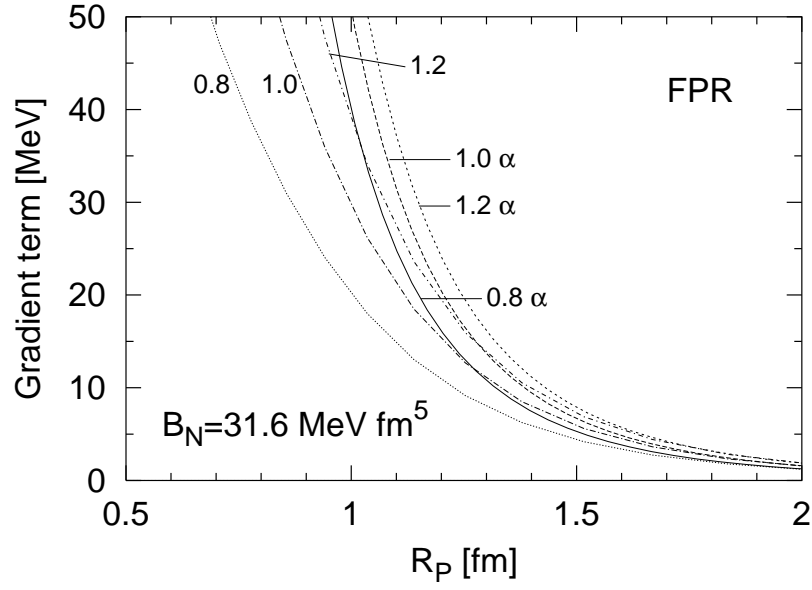


Fig. 10. The same as in Fig.9 for the Friedman-Pandharipande-Ravenhall interactions.



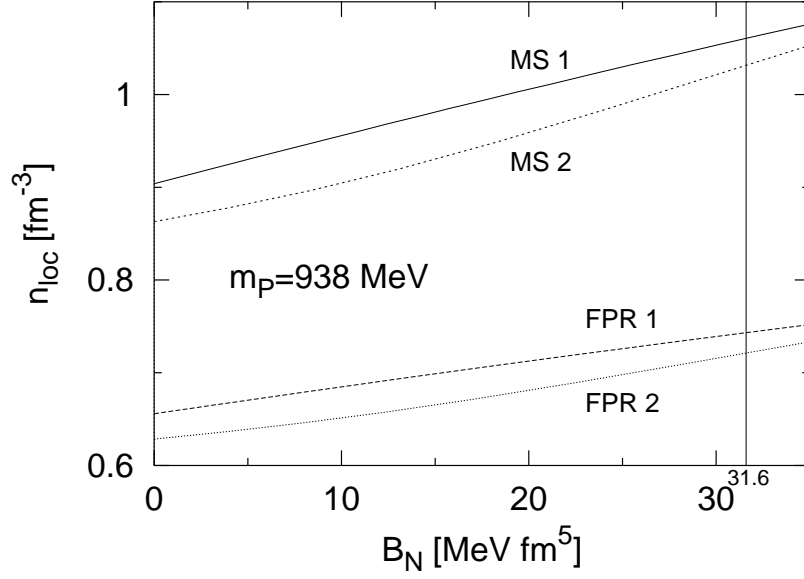


Fig. 11. The threshold density for proton localization versus the curvature coefficient  $B_N$ . The curves MS1 and FPR1 correspond to the simple method of Sect.3. The curves MS2 and FPR2 correspond to the self-consistent calculations.

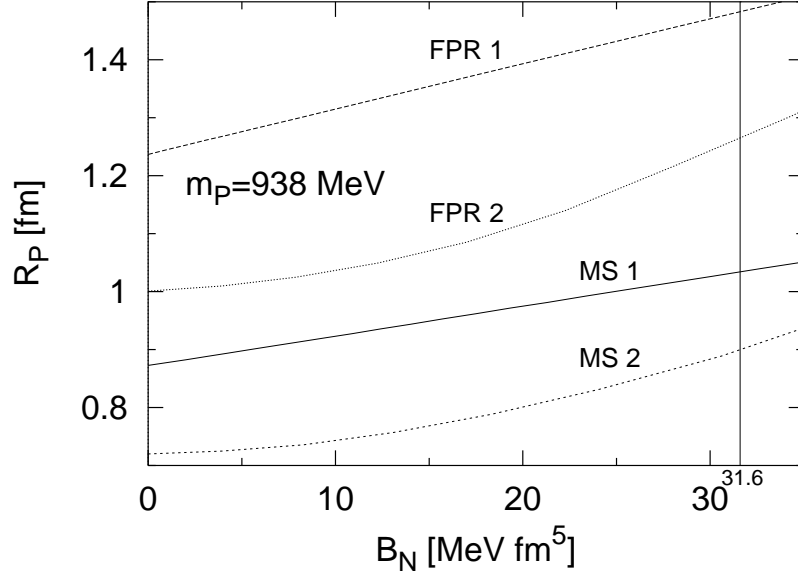


Fig. 12. The rms proton distribution radius at the threshold density as a function of the curvature coefficient  $B_N$ . Curves labeled as in Fig.11

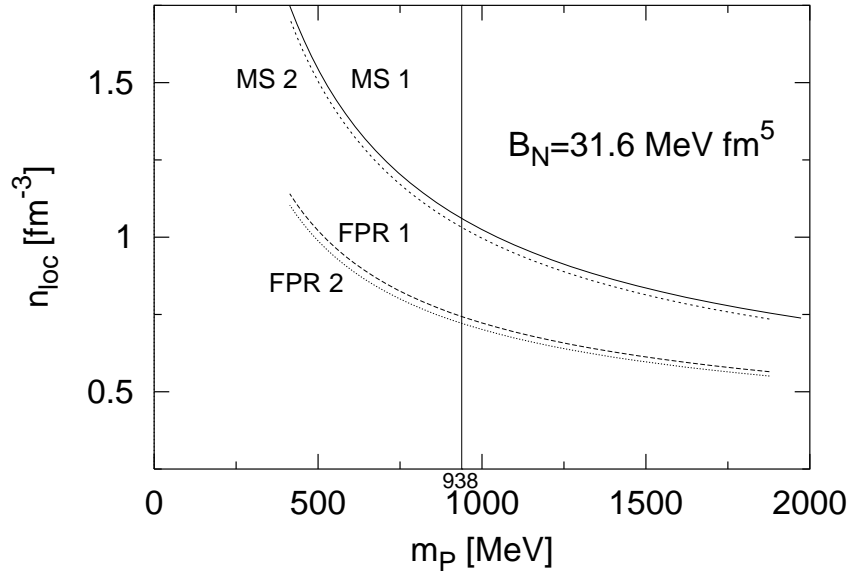


Fig. 13. The threshold density for proton localization as a function of the proton effective mass. Curves labeled as in Fig.11

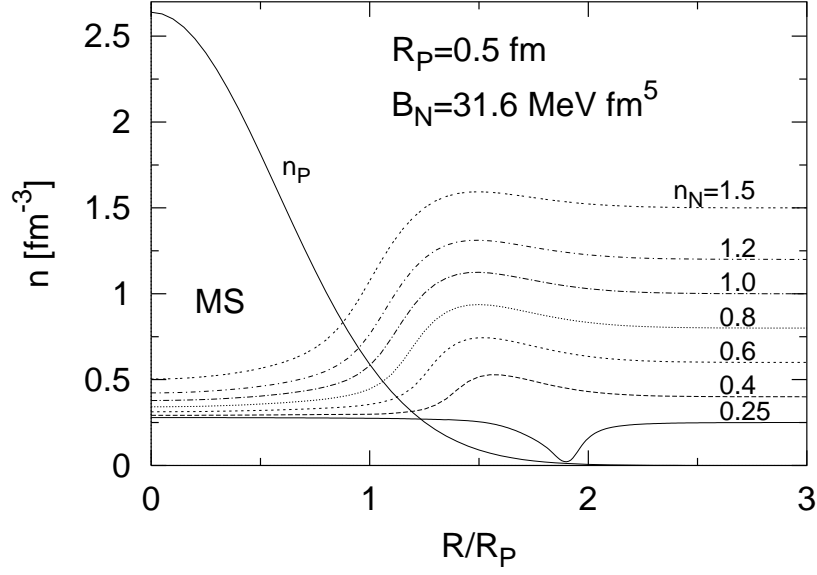


Fig. 14. The neutron density distribution obtained from Eq.(16) for indicated neutron matter densities (in  $\text{fm}^{-3}$ ) for the Myers and Swiatecki interactions. The localized proton distribution  $n_P$  is also shown.

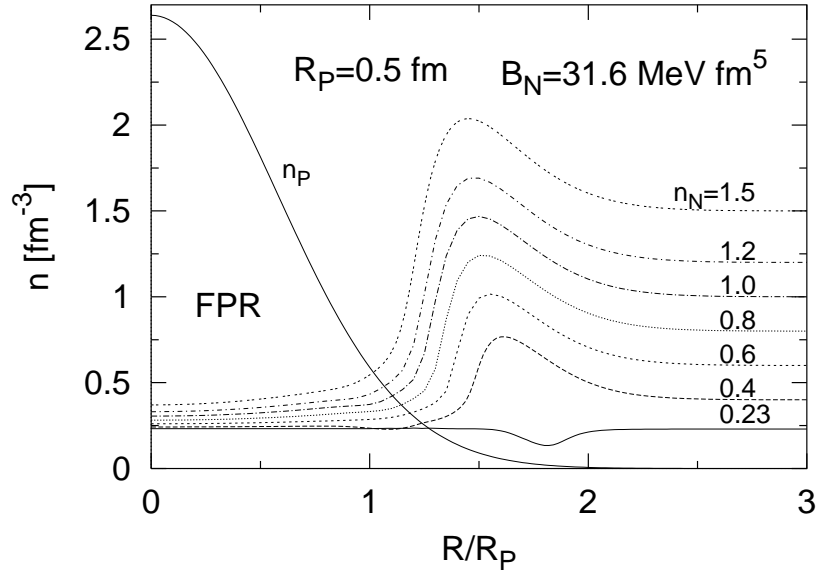


Fig. 15. The same as in Fig.14 for the Friedman-Pandharipande-Ravenhall interactions.

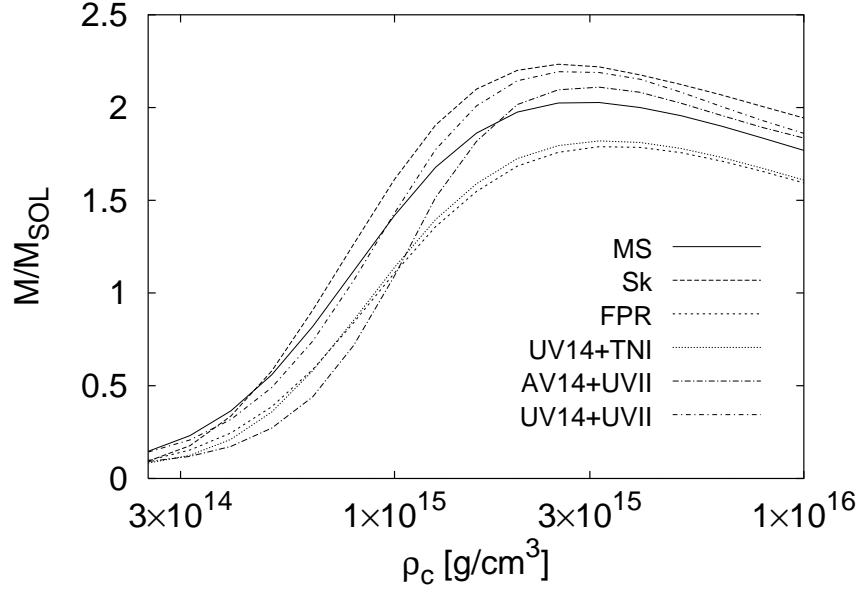


Fig. 16. Neutron star masses (in solar units) as functions of the central density for nuclear interaction models from Fig.1.